Fermi level unpinning of GaSb (100) using plasma enhanced atomic layer deposition of Al_2O_3

A. Ali,[1,a] H. S. Madan,[1] A. P. Kirk,[2] D. A. Zhao,[1] D. A. Mourey,[1] M. K. Hudait,[3] R. M. Wallace,[2] T. N. Jackson,[1] B. R. Bennett,[4] J. B. Boos,[4] and S. Datta[1]
[1]*Penn State University, University Park, Pennsylvania 16802, USA*
[2]*The University of Texas at Dallas, Richardson, Texas 75080, USA*
[3]*Virginia Tech, Blacksburg, Virginia 24061, USA*
[4]*Naval Research Laboratory, Washington, DC 20375, USA*

(Received 14 May 2010; accepted 2 September 2010; published online 4 October 2010)

N-type and p-type GaSb metal-oxide-semiconductor capacitors (MOSCAPs) with atomic-layer-deposited (ALD) and plasma-enhanced-ALD (PEALD) Al_2O_3 dielectrics are studied to identify the optimum surface preparation and oxide deposition conditions for a high quality oxide-semiconductor interface. The ALD Al_2O_3/GaSb MOSCAPs exhibit strongly pinned C-V characteristics with high interface state density (D_{it}) whereas the PEALD Al_2O_3/GaSb MOSCAPs show unpinned C-V characteristics (low D_{it}). The reduction in Sb_2O_3 to metallic Sb is suppressed for the PEALD samples due to lower process temperature, identified by x-ray photoelectron spectroscopy analysis. Absence of elemental Sb is attributed to unpinning of Fermi level at the PEALD Al_2O_3/GaSb interface. © *2010 American Institute of Physics*. [doi:10.1063/1.3492847]

Antimonide based compound semiconductors have gained considerable interest in recent years due to their superior electron and hole transport properties.[1,2] Mixed anion $InAs_xSb_{1-x}$ quantum-wells (QWs) with high electron mobility are candidates for integration with high hole mobility $In_xGa_{1-x}Sb$ QW for low power complementary logic applications.[3] Recently, $InAs/Al_yGa_{1-y}Sb$ heterojunction tunnel field effect transistors (H-TFETs) have been proposed for low-power high-performance applications.[4] Integrating a high quality dielectric is key to demonstrating a scalable metal-oxide-semiconductor QWFET (MOS-QWFET) or H-TFET architecture for low-power logic applications. We hypothesize that an ultrathin GaSb surface layer is more favorable toward high-κ dielectric integration than $Al_yIn_{1-y}Sb$ barrier layer for the QWFET or $Al_yGa_{1-y}Sb$ channel layer for the H-TFET, as it avoids Al at the interface and the associated surface oxidation. Hence, it is imperative to carefully examine the electrical characteristics of high-κ/GaSb semiconductor interface.

GaSb has a highly reactive surface and on exposure to air it will form a native oxide layer composed of Ga_2O_3 and Sb_2O_3 ($2GaSb+3O_2 \rightarrow Ga_2O_3+Sb_2O_3$). The Sb_2O_3 can further react with the GaSb surface forming elemental Sb and Ga_2O_3 ($Sb_2O_3+2GaSb \rightarrow Ga_2O_3+4Sb$).[5,6] Chemical treatments based on HCl are effective in removing native oxides on GaSb.[6,7] Here, we study the effects of HCl treatment on the capacitance-voltage characteristics (C-V) and the surface chemistry of n-type and p-type GaSb(100) MOS capacitors fabricated with both atomic-layer-deposited (ALD) and plasma enhanced ALD (PEALD) Al_2O_3 dielectrics. PEALD was employed to reduce the thermal budget of dielectric deposition, particularly important for antimonide based semiconductors. In this Letter, we demonstrate an unpinned Fermi level in GaSb MOS system with a high-κ PEALD Al_2O_3 dielectric, using temperature resolved admittance spectroscopy and monochromatic x-ray photoelectron spectroscopy (XPS) analysis.

Both n-type and p-type GaSb (100) MOS capacitors were fabricated with high-κ Al_2O_3 gate dielectric. The samples were degreased in acetone and ethanol for 5 min each and rinsed in isopropyl alcohol (IPA). The degrease step was followed by a dip in concentrated HCl ($HCl:H_2O=1:2$) for 5 min to remove surface oxides followed by an IPA rinse. GaSb MOS capacitors were fabricated with Al_2O_3 deposited by ALD at 300 °C from trimethylaluminum (TMA) and water or by PEALD at 200 °C from TMA and CO_2.[8] Pt/Au gate metallization was done using electron beam evaporation after defining gate patterns using optical lithography. Pd/Au backside Ohmic contacts were deposited using electron beam evaporation. No post deposition anneal was done for any of the samples.

Capacitance voltage (C-V) and conductance voltage (G-V) measurements were obtained with HP 4285A precision *LCR* meter. Figure 1(a) shows the C-V measurements on ALD Al_2O_3/n-GaSb and PEALD Al_2O_3/n-GaSb MOS capacitors. The ALD sample shows weakly pinned C-V characteristics with very fast interface trap density (D_{it}) response whereas PEALD sample demonstrates good Fermi level modulation. The accumulation side of C-V characteristics for the PEALD sample shows the effect of high D_{it} near the conduction band (CB) and the negative bias regime shows the effect of inversion response along with a low D_{it} response. The accumulation side of the admittance data is analyzed using the standard depletion/accumulation model[9] and the inversion side using an alternative.[10] The circuit model in inversion accounts for the supply of minority carriers through bulk thermal generation and diffusion across the space charge layer along with interface state contribution, which enables accurate modeling of the admittance data in inversion. Figure 1(b) shows C-V characteristics of the ALD Al_2O_3/p-GaSb and PEALD Al_2O_3/p-GaSb samples with HCl treatment for different temperatures. The ALD sample shows strongly pinned C-V characteristics with both accumulation and inversion regimes completely dominated by interface states. For the PEALD sample, there is minimal dispersion of capacitance in accumulation due to less D_{it} near

[a]Electronic mail: aua176@psu.edu.

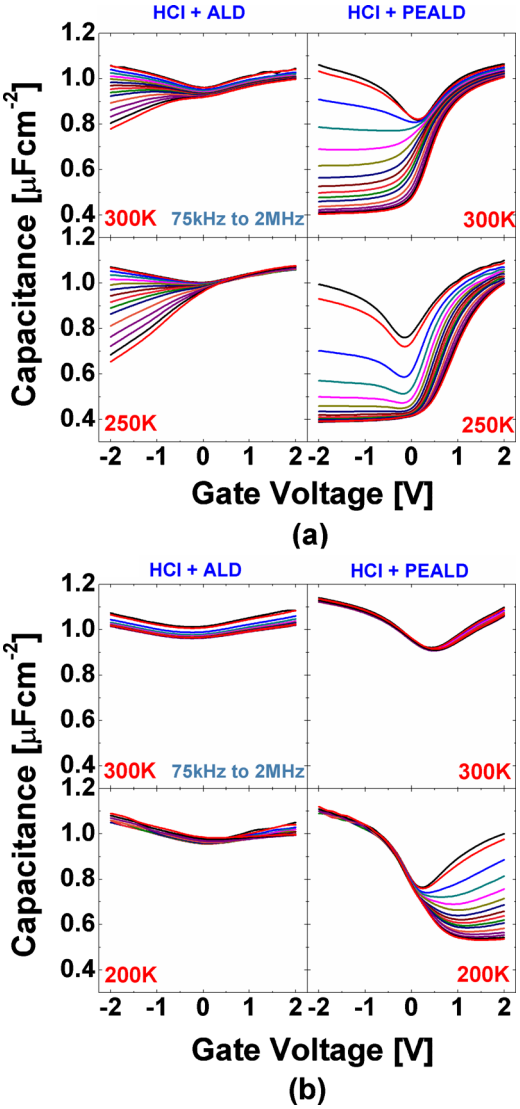

FIG. 1. (Color online) C-V characteristics as a function of frequency of (a) n-type ALD and PEALD samples with HCl treatment and (b) p-type ALD and PEALD samples with HCl treatment. Measurement temperature is indicated in the figure.

the valence band (VB) whereas the inversion response shows contributions from minority carriers as well as high D_{it} near the CB. The 200 K C-V shows a clear Fermi level movement from accumulation to depletion for the PEALD sample whereas ALD sample exhibits pinned C-V characteristics. C-V measurements for the n-type (p-type) MOS capacitors were done at 300 and 250 K (300 and 200 K). The reason is that the backside contact (Pd/Au) on GaSb is Ohmic for holes whereas it forms a Schottky barrier for electrons (~0.6 eV Schottky barrier height for electrons due to the Fermi stabilization energy in GaSb being ~0.1 eV from the VB.[11] This Schottky barrier gives rise to higher contact resistance for electrons at lower temperatures, which causes frequency dispersion in the accumulation capacitance of the n-type metal-oxide-semiconductor capacitors (MOSCAPs). For the p-type devices this is not a problem as the contacts are Ohmic for holes, and the measurement can be done at very low temperature. Hence, the above measurement temperatures were employed.

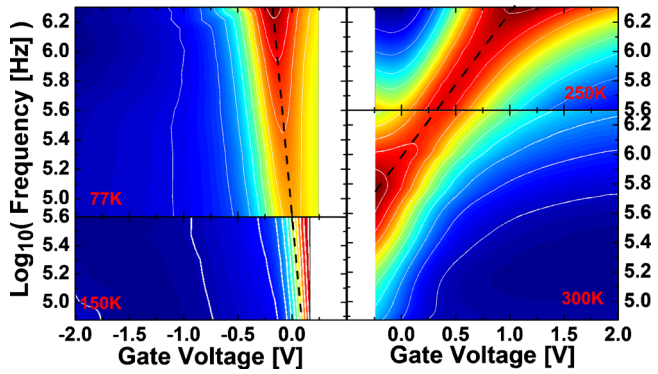

FIG. 2. (Color online) Conductance (G/ω) contours of n-type and p-type GaSb MOSCAPs with PEALD Al_2O_3 showing good Fermi level modulation toward valence and conduction band sides.

Figure 2 shows the conductance contour map (G/ω) of n-type and p-type PEALD samples as a function of gate voltage and small-signal frequency. The V-shaped trajectory of the peak value of conductance, $(G/\omega)_{peak}$, along the frequency axis shows that the Fermi level moves freely on either side of the midgap of GaSb. PEALD Al_2O_3/GaSb samples demonstrate an unpinned Fermi level at the interface, even though the Fermi stabilization energy for GaSb is 0.1 eV from the VB.[11] The extracted capture cross section values are 9×10^{-15} cm^2 for traps near the VB and 8×10^{-19} cm^2 for traps near the CB, indicating that the traps near the VB are faster than those near the CB. Hence, the conductance plots were done at lower temperature for the p-type samples where the conductance peaks were visible. The capture cross section values are consistent with Ref. 12, where irradiated p-type GaSb showed acceptor type traps near the VB with higher capture cross-section.

Figure 3 shows the monochromatic XPS analysis of the Sb 4*d* region for the ALD and PEALD samples with HCl treatment.[13] All PEALD and ALD samples show presence of Ga-oxides. The ALD samples show no detectable Sb-oxides where as the PEALD samples have significant Sb-oxides. As

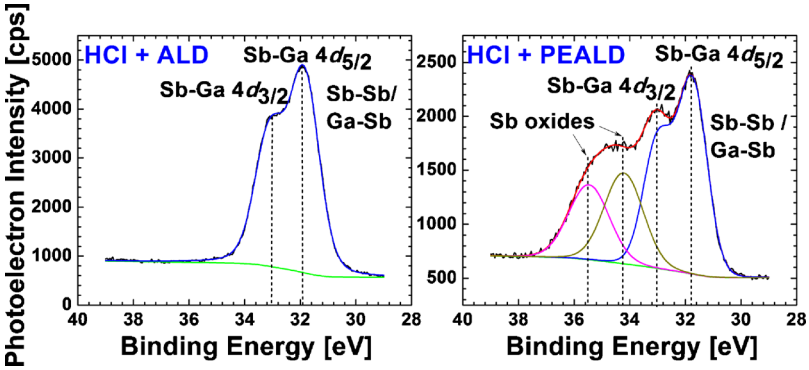

FIG. 3. (Color online) XPS data comparing the concentration of Sb_2O_3 in ALD and PEALD samples. Reduction in Sb_2O_3 in the (higher temperature) ALD samples is evident.

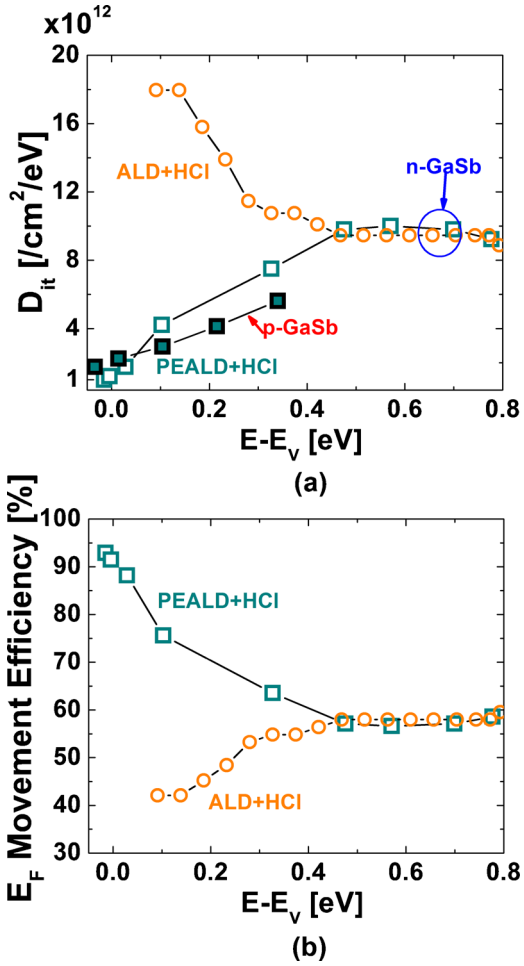

FIG. 4. (Color online) (a) Extracted D_{it} from n-type and p-type samples showing low D_{it} near VB for PEALD MOSCAPs. The inversion side for the n-type MOSCAPs was modeled to evaluate D_{it} (Ref. 9) which is consistent with the data obtained from p-type samples. (b) Fermi level movement efficiency of GaSb MOSCAPs with ALD and PEALD Al_2O_3.

mentioned before, Sb_2O_3 reacts with GaSb forming Ga_2O_3 and elemental Sb.[6] The kinetics of this reaction is enhanced at higher temperatures >200 °C.[14] Enhanced thermal desorption of Sb-oxides are also anticipated at such temperatures.[15] The ALD, which was done at 300 °C, could therefore result in significant formation of elemental Sb, thereby reducing the available Sb_2O_3. In contrast, the PEALD was done at 200 °C where the reduction is significantly suppressed. The 4*d* orbital binding energy of elemental Sb (Sb–Sb) is similar to that for GaSb. Hence, due to the Al_2O_3 thickness, it is difficult to conclude whether the PEALD samples are free from elemental Sb. It is possible that the Fermi level, E_F, unpinning for PEALD samples is due to the absence of elemental Sb at the Al_2O_3/GaSb interface. Further, the absence of water in PEALD, coupled with low thermal budget, leads to a better quality interface. Finally, F was detected in all samples by XPS and is attributed to reactor O-ring decomposition. The role of F remains a topic of investigation. We have also studied the C-V characteristics of GaSb samples with ALD Al_2O_3 deposited at 200 °C. The C-V characteristics (not shown here) showed better gate modulation (i.e., higher C_{max}/C_{min} ratio) compared to the 300 °C ALD sample. This is due to the reduced amount of elemental Sb formation at 200 °C. However the 200 °C ALD sample still exhibits high D_{it} toward VB side of GaSb, and is inferior to the 200 °C PEALD sample. We also speculate that the oxide anions in the plasma during the PEALD process may more efficiently oxidize the elemental Sb back to Sb_2O_3.

Figure 4(a) shows the D_{it} extracted from the n-type and p-type samples. The D_{it} extracted from the n-type MOSCAP data using the inversion mode model (Ref. 9) is consistent with the analysis on the p-type sample. Figure 4(b) shows the Fermi level movement efficiency of the ALD and PEALD samples. Fermi level movement efficiency is defined as the ratio of the change in the Fermi level at the oxide-semiconductor interface in the presence of D_{it} to the change in Fermi level without D_{it}, for a unit applied gate voltage. Mathematically, it can be represented as follows:

$$E_F \text{ movement efficiency} = \frac{1 + C_{dep}/C_{ox}}{1 + (C_{dep} + C_{it})/C_{ox}}\%. \quad (1)$$

The PEALD sample with HCl pretreatment shows a 90% E_F movement efficiency near the VB making it suitable for MOS-QWFET or H-TFET device operations, where the Fermi level sweeps near the VB of GaSb.

In summary, we have demonstrated GaSb MOS capacitors (p-type and n-type) with unpinned Fermi level using PEALD Al_2O_3 by minimizing elemental Sb at the GaSb/Al_2O_3 interface. The reduction of Sb_2O_3 to metallic Sb is suppressed with PEALD due to lower deposition temperature, which is confirmed by XPS analysis. The D_{it} is low near the valence band which makes GaSb-PEALD Al_2O_3 a good interface for composite barrier design with $Al_yIn_{1-y}Sb$ and $Al_yGa_{1-y}Sb$ barrier layers in mixed-anion MOS-QWFETs or H-TFETs for ultralow power logic applications.

Some of the authors gratefully acknowledge the financial support from the FCRP for Materials, Structures, and Devices (MSD) sponsored by the SRC and DARPA.

[1] S. Datta, T. Ashley, J. Brask, L. Buckle, M. Doczy, M. Emeny, D. Hayes, K. Hilton, R. Jefferies, T. Martin, T. Phillips, D. Wallis, P. Wilding, and R. Chau, Tech. Dig. - Int. Electron Devices Meet. **2005**, 763.
[2] M. Radosavljevic, T. Ashley, A. Andreev, S. D. Coomber, G. Dewey, M. T. Emeny, M. Fearn, D. G. Hayes, K. P. Hilton, M. K. Hudait, R. Jefferies, T. Martin, R. Pillarisetty, W. Rachmady, T. Rakshit, S. J. Smith, M. J. Uren, D. J. Wallis, P. J. Wilding, and R. Chau, Tech. Dig. - Int. Electron Devices Meet. **2008**, 727.
[3] B. P. Tinkham, B. R. Bennett, R. Magno, B. V. Shanabrook, and J. B. Boos, J. Vac. Sci. Technol. B **23**, 1441 (2005).
[4] J. Knoch and J. Appenzeller, IEEE Electron Device Lett. **31**, 305 (2010).
[5] P. S. Dutta, H. L. Bhat, and V. Kumar, J. Appl. Phys. **81**, 5821 (1997).
[6] G. P. Schwartz, G. J. Gualtieri, J. E. Griffiths, C. D. Thurmond, and B. Schwartz, J. Electrochem. Soc. **127**, 2488 (1980).
[7] C. L. Lin, Y. K. Su, T. S. Se, and W. L. Li, Jpn. J. Appl. Phys., Part 2 **37**, L1543 (1998).
[8] D. A. Mourey, D. A. Zhao, J. Sun, and T. N. Jackson, IEEE Trans. Electron Devices **57**, 530 (2010).
[9] A. Ali, H. Madan, S. Koveshnikov, S. Oktyabrsky, R. Kambhampati, T. Heeg, D. Schlom, and S. Datta, IEEE Trans. Electron Devices **57**, 742 (2010).
[10] Y. Fukuda, Y. Otani Y. Itayama, and T. Ono, IEEE Trans. Electron Devices **54**, 2878 (2007).
[11] W. Walukiewicz, Phys. Rev. B **37**, 4760 (1988).
[12] R. Kaiser and H. Y. Fan, Phys. Rev. **138**, A156 (1965).
[13] Details of the XPS analysis system are described in: R. M. Wallace, ECS Trans. **16**(5), 255 (2008).
[14] C. J. Vineis, C. A. Wang, and K. F. Jensen, J. Cryst. Growth **225**, 420 (2001).
[15] Z. Y. Liu, B. Hawkins, and T. F. Kuech, J. Vac. Sci. Technol. B **21**, 71 (2003).